Supporting Information

Nanophase-Separation in Immiscible Double-Network Elastomers Induces Synergetic Strengthening, Toughening, and Fatigue-Resistance

Yong Zheng[1], Ryuji Kiyama[1], Takahiro Matsuda[2], Kunpeng Cui[4], Wei Cui[3], Xueyu Li[3], Yunzhou Guo[1], Tasuku Nakajima[2,3,4]*, Takayuki Kurokawa[2,3], and Jian Ping Gong[2,3,4]*

[1]*Graduate School of Life Science, Hokkaido University, Sapporo 001-0021, Japan*

[2]*Faculty of Advanced Life Science, Hokkaido University, Sapporo 001-0021, Japan*

[3]*Global Station for Soft Matter, Global Institution for Collaborative Research and Education (GI-CoRE), Hokkaido University, Sapporo 001-0021, Japan*

[4]*Institute for Chemical Reaction Design and Discovery (WPI-ICReDD), Hokkaido University, Sapporo 001-0021, Japan*

*Corresponding author: tasuku@sci.hokudai.ac.jp; gong@sci.hokudai.ac.jp

Table S1. Mechanical properties of DN elastomers and gels.

	E (MPa)	λ_b (mm/mm)	σ_b (MPa)	λ_y (mm/mm)	σ_y (MPa)	W_b (MJ m^{-3})	T (kJ m^{-2})	φ_{1st} (vol%)	T_g (°C)
DN-0 elastomer	0.15	6.0	2.6	-	-	4.8	-	20.4	-34.6
DN-0.1 elastomer	0.14	8.5	1.6	4.8	1.4	9.5	2.0	4.5	-34.7
DN-0.5 elastomer	0.43	6.6	2.0	3.5	2.3	8.9	6.2	4.1	-
DN-0.9 elastomer	0.91	9.0	2.8	3.0	3.1	19.5	8.2	2.8	-36.2
DN-1.0 elastomer	1.83	6.4	3.5	3.1	4.3	22.0	10.8	5.1	-33.9
S_2N elastomer	0.08	13.2	0.4	-	-	1.9	0.5	-	-35.0
DN-0 gel	0.06	4.8	0.6	-	-	0.6	-	-	-
DN-0.1 gel	0.08	4.0	1.0	3.4	1.1	1.4	0.2	-	-
DN-0.5 gel	0.10	3.1	1.4	3.0	1.6	1.1	0.3	-	-
DN-0.9 gel	0.11	3.0	1.4	2.8	1.6	1.2	-	-	-
DN-1.0 gel	0.14	3.0	2.1	3.0	2.1	1.6	0.4	-	-

Young's modulus (E), elongation ratio and nominal stress at yielding (λ_y and σ_y, respectively), elongation ratio, nominal stress and input energy density at break (λ_b, σ_b and W_b, respectively), fracture energies characterized by trouser-shaped tearing (T) and glass transition temperature (T_g) are summarized. The volume ratio of first network in DN elastomer φ_{1st} is calculated from $\varphi_{1st} = (\frac{h_{1st}}{h_{DN}})^3$, where h_{1st} and h_{DN} are the thickness of dried first network and DN elastomer, respectively.

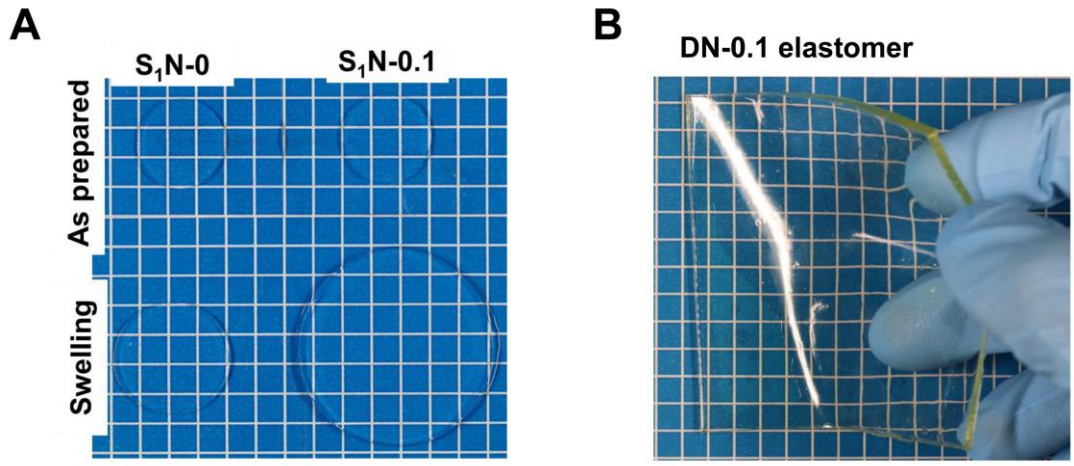

Figure S1. (A) Swelling comparison of S_1N prepared with and without electrolyte component in second monomer solution (4.7 M MEA in organic solvent NMF). S_1N-0 and S_1N-0.1 represent S_1N synthesized without any AMPS and with 10% AMPS in feed monomer concentration, respectively. (B) Digital photo of DN-0.1 elastomer.

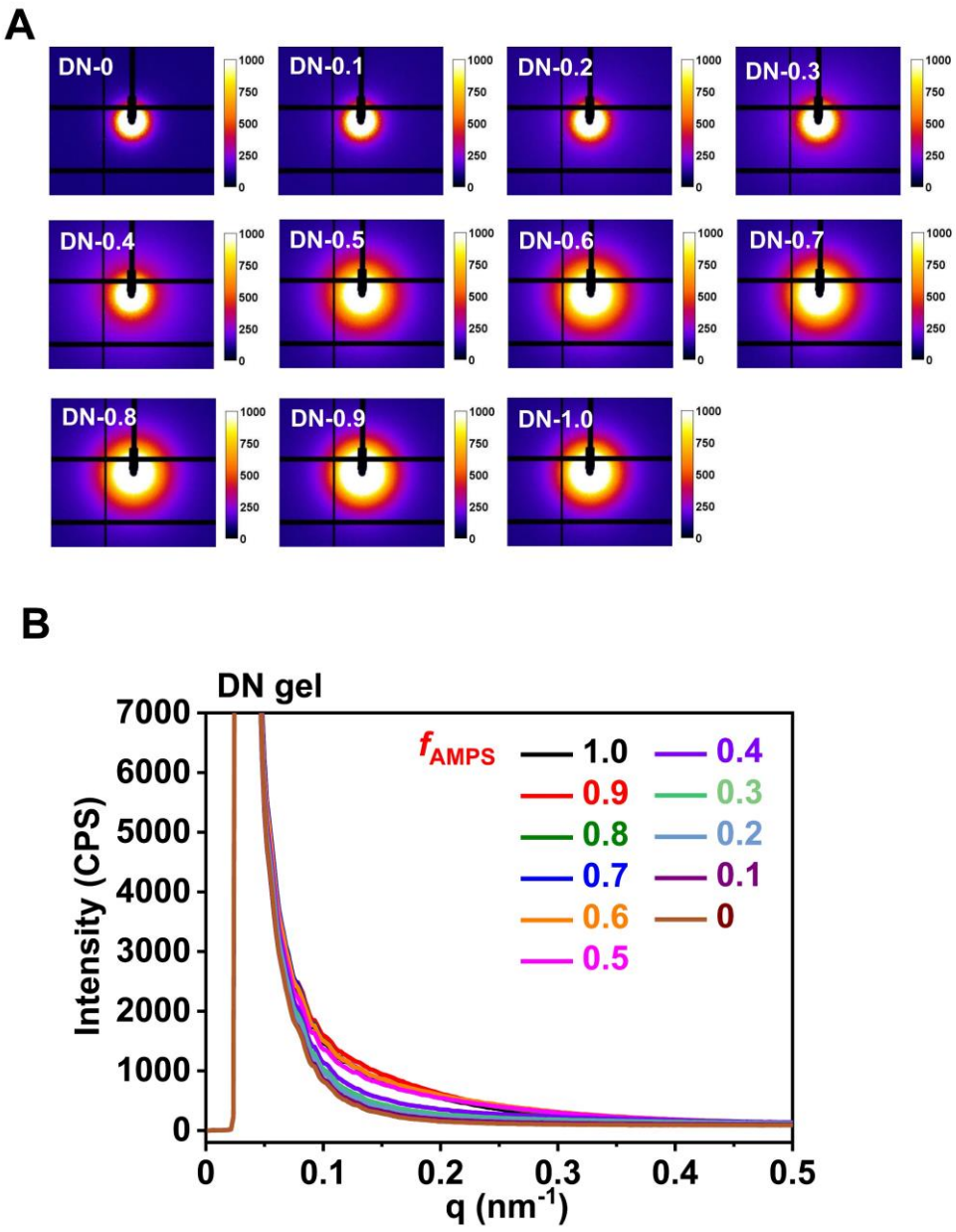

Figure S2. SAXS results of DN gels. (A) 2D SAXS patterns and (B) corresponding 1D scattering intensity profiles of DN gels prepared with various f_{AMPS} molar ratios ranging from 0 to 1.0. No phase-separated structure is formed in these DN-f_{AMPS} gels.

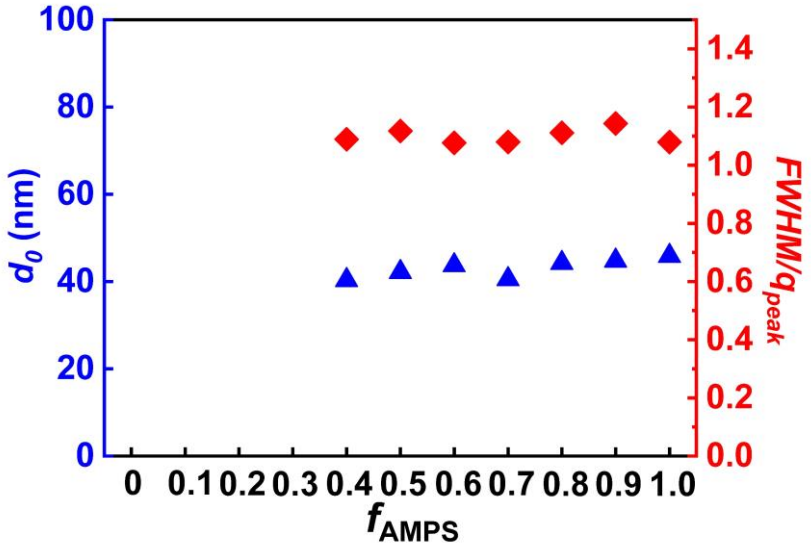

Figure S3. Domain spacing d_0 and $FWHM/q_{peak}$ of DN-f_{AMPS} elastomers plotted as functions of f_{AMPS} molar fraction.

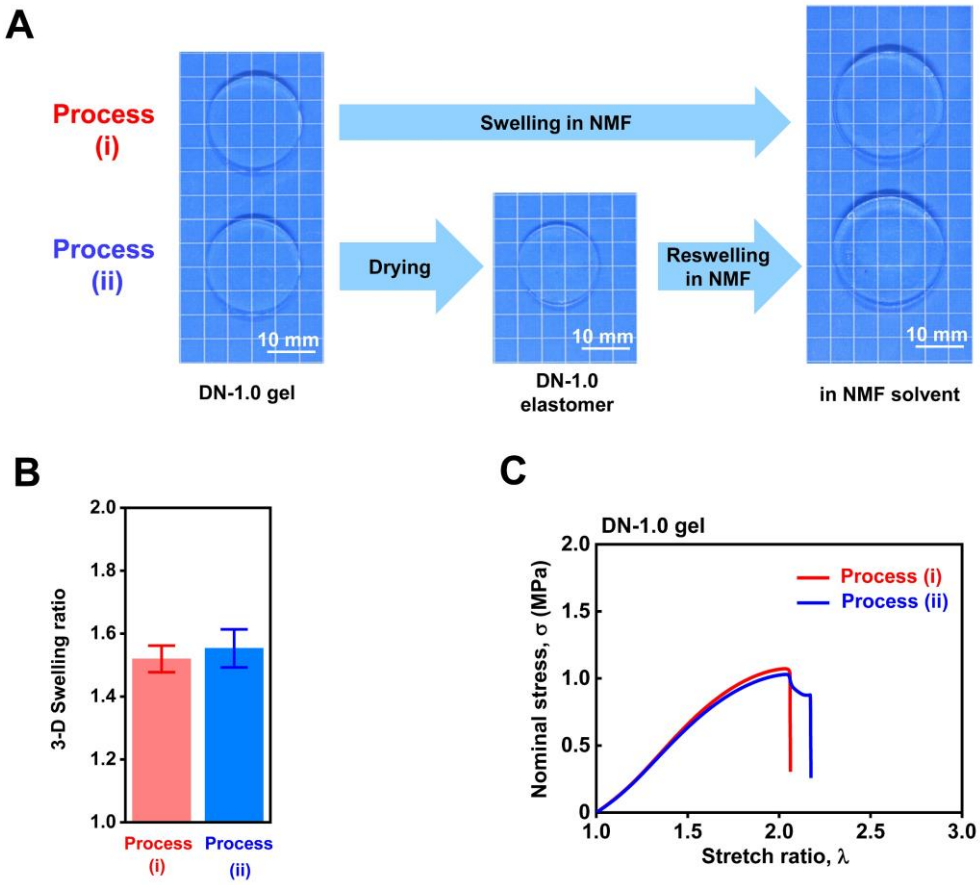

Figure S4. Reswelling of DN-1.0 elastomer in NMF. (A) Two swelling processes and (B) corresponding three-dimensional swelling ratios. Processes (i) and (ii) denote direct swelling of DN-1.0 gel and reswelling of dried DN-1.0 elastomer both in NMF, respectively. (C) Tensile curves of DN-1.0 gels for Processes (i) and (ii). Reswelling ratio and tensile behavior of DN-1.0 elastomer are identical to those of corresponding original DN-1.0 gel, confirming that phase separation does not damage double-network structure.

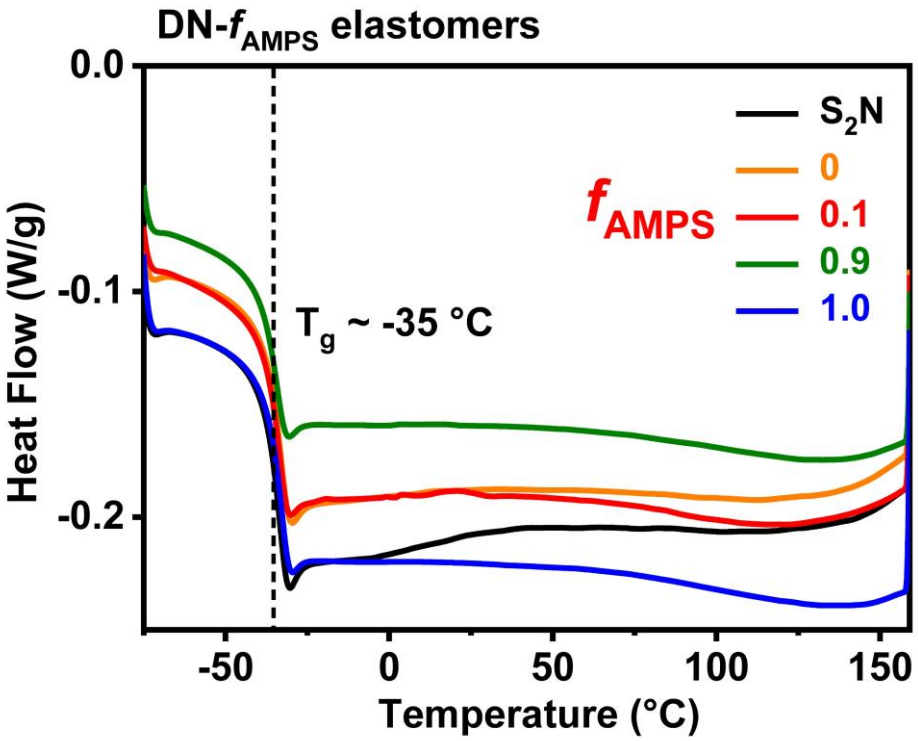

Figure S5. DSC thermograms of DN elastomers generated at 10 K min^{-1}. All DN elastomers show same glass-transition temperature T_g around −35 °C, corresponding to glass transition of nonpolar PMEA. The testing sample was pre-equilibrated at −70 °C for 10 min and then was heated at a rate of 10 K/min, and measurement was performed from –70 to 160 °C using air as a reference.

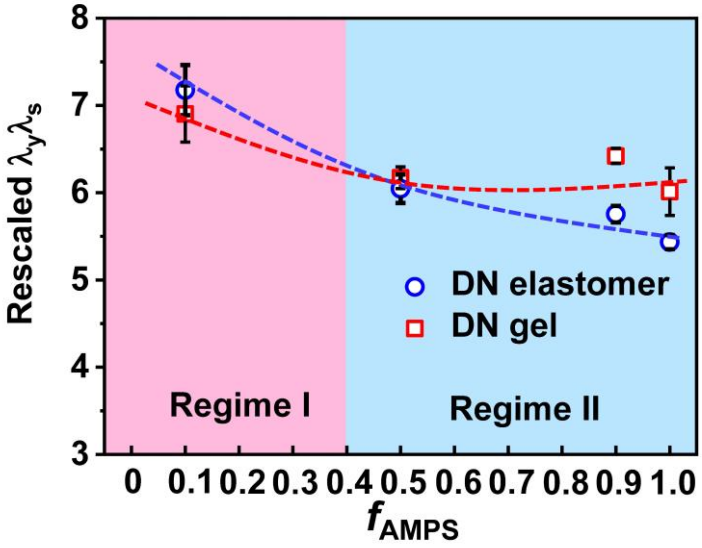

Figure S6. Rescaled yielding stretch ratio $\lambda_y\lambda_s$ of DN gels and elastomers plotted as functions of f_{AMPS}. In regimes I and II, DN elastomers did not show any and showed obvious phase separation, respectively.

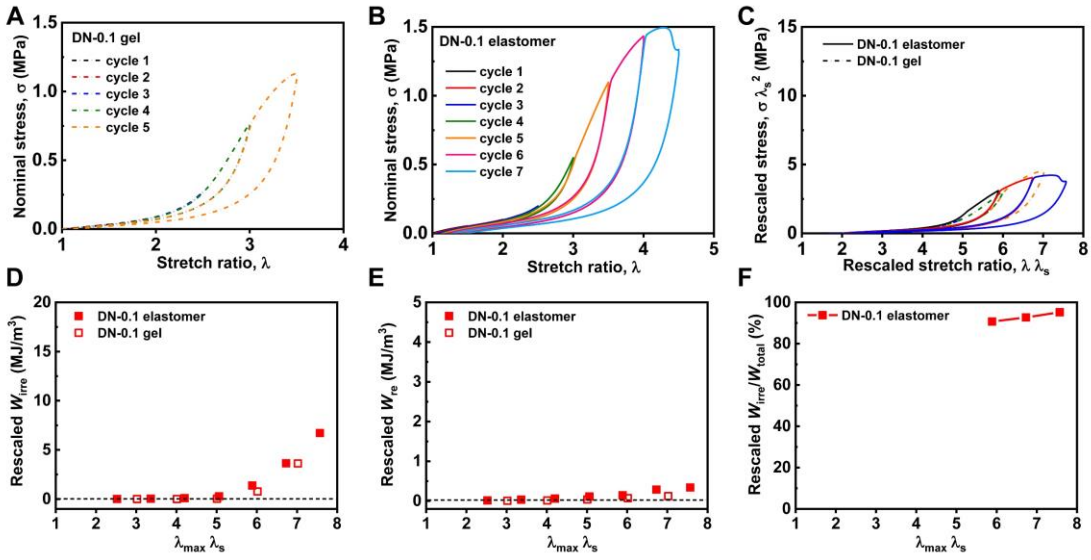

Figure S7. Comparison of rescaled energy-dissipation behaviors of DN-0.1 elastomer and corresponding gel, as studied by cyclic tensile tests. (A, B) Sequential loading–unloading cycles for DN-0.1 (A) gel and (B) elastomer. (C) Rescaled loading–unloading cycles for DN-0.1 gel and corresponding elastomer. (D–F) Rescaled (D) irreversible dissipation (W_{irre}), (E) reversible hysteresis (W_{re}), and (F) irreversible ratio (W_{irre}/W_{total}) for DN-0.1 elastomer. For comparison, data for DN-0.1 gel are also shown. The cyclic loading-unloading is performed with a strain rate of 0.14 s^{-1} and without waiting time between cycles.

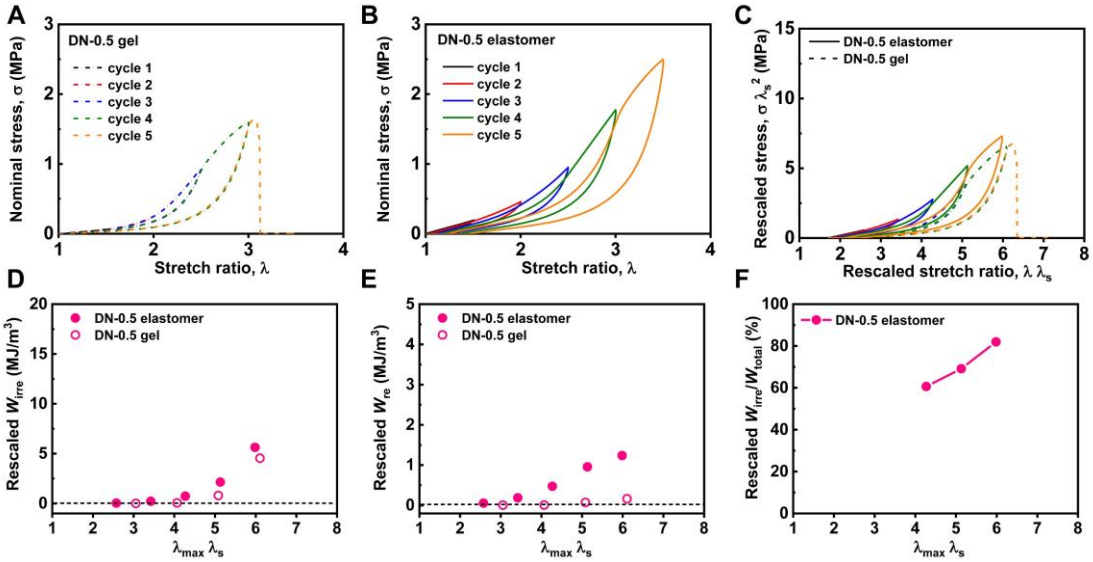

Figure S8. Comparison of rescaled energy-dissipation behaviors of DN-0.5 elastomer and corresponding gel, as studied by cyclic tensile tests. (A, B) Sequential loading–unloading cycles for DN-0.5 (A) gel and (B) elastomer. (C) Rescaled loading–unloading cycles for DN-0.5 gel and corresponding elastomer. (D–F) Rescaled (D) irreversible dissipation (W_{irre}), (E) reversible hysteresis (W_{re}), and (F) irreversible ratio (W_{irre}/W_{total}) for DN-0.5 elastomer. For comparison, data for DN-0.5 gel are also shown. The cyclic loading-unloading is performed with a strain rate of 0.14 s^{-1} and without waiting time between cycles.

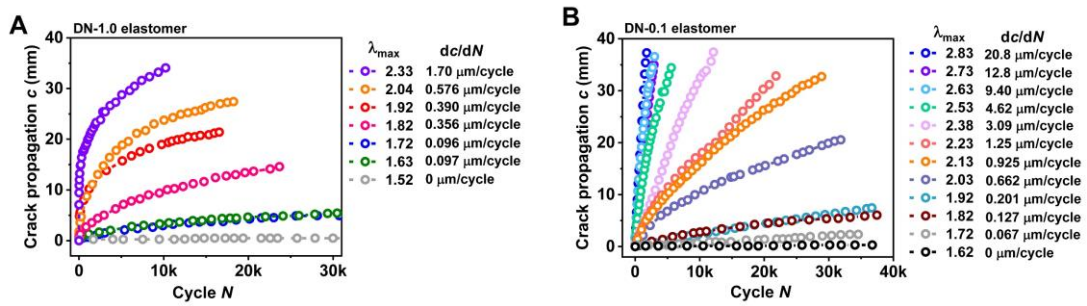

Figure S9. Crack propagation length *c* as a function of the number of cycles *N* with different applied stretch ratio λ_{max} for DN-1.0 and DN-0.1 elastomers. (A) For DN-1.0 elastomer, the crack propagation length *c* initially increases fast, but crack growth slows down soon to a much slower crack propagation rate with increasing cycle *N*. The average crack propagation rate at steady state d*c*/d*N* is the slope of *c* versus *N* plot taken after 5000th cycles where the crack propagation reaches steady state. (B) For DN-0.1 elastomer, the crack propagation length *c* increases at a stable rate from initial stage. At $\lambda_{max} < 2.38$, the d*c*/d*N* is taken after 5000th cycles. At $\lambda_{max} > 2.38$, d*c*/d*N* is taken after 200th cycles.

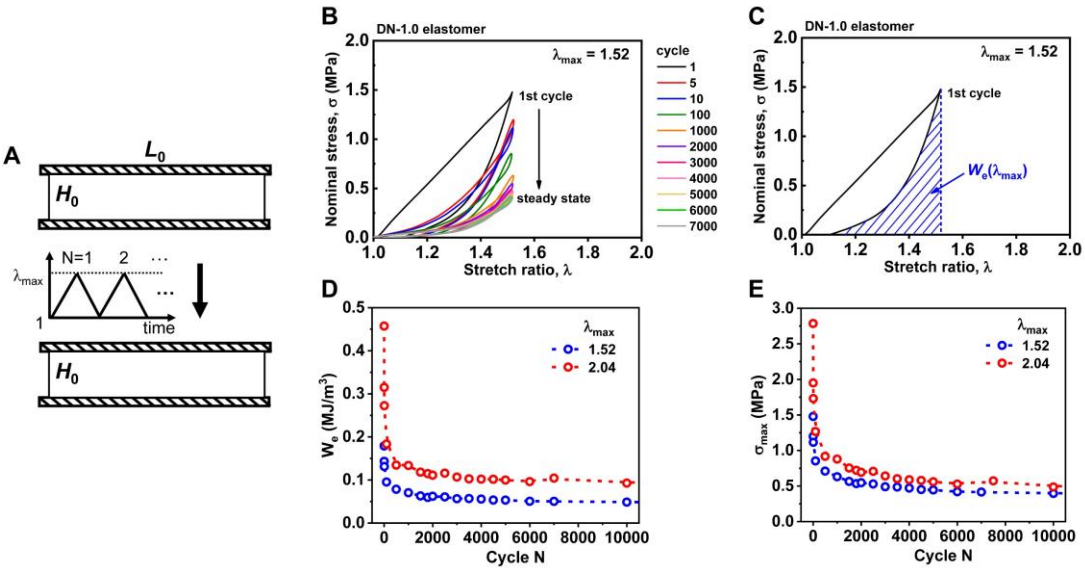

Figure S10. Experimental set-up and characterizing the energy release rate G for DN-1.0 elastomer. (A) Schematic of the experimental set-up. (B) The loading-unloading curves to λ_{max} with increasing cycle N. The curves drop greatly at the beginning of the cycles and reach a steady state after thousands of cycles. (C) The area under the unloading curve shown by the blue hatch represents the elastic strain energy density $W_e(\lambda_{max})$. (D) Evolution of $W_e(\lambda_{max})$ and (E) σ_{max} with cycle N. The λ_{max}=1.52 and 2.04 are shown as examples. The $W_e(\lambda_{max})$ drops greatly at the beginning cycles and reaches a steady state after 2000 cycles. $W_e(\lambda_{max})$ at the 5000th cycle is used to estimate the energy release rate G by $G = W_e(\lambda_{max}) \times H_0$.

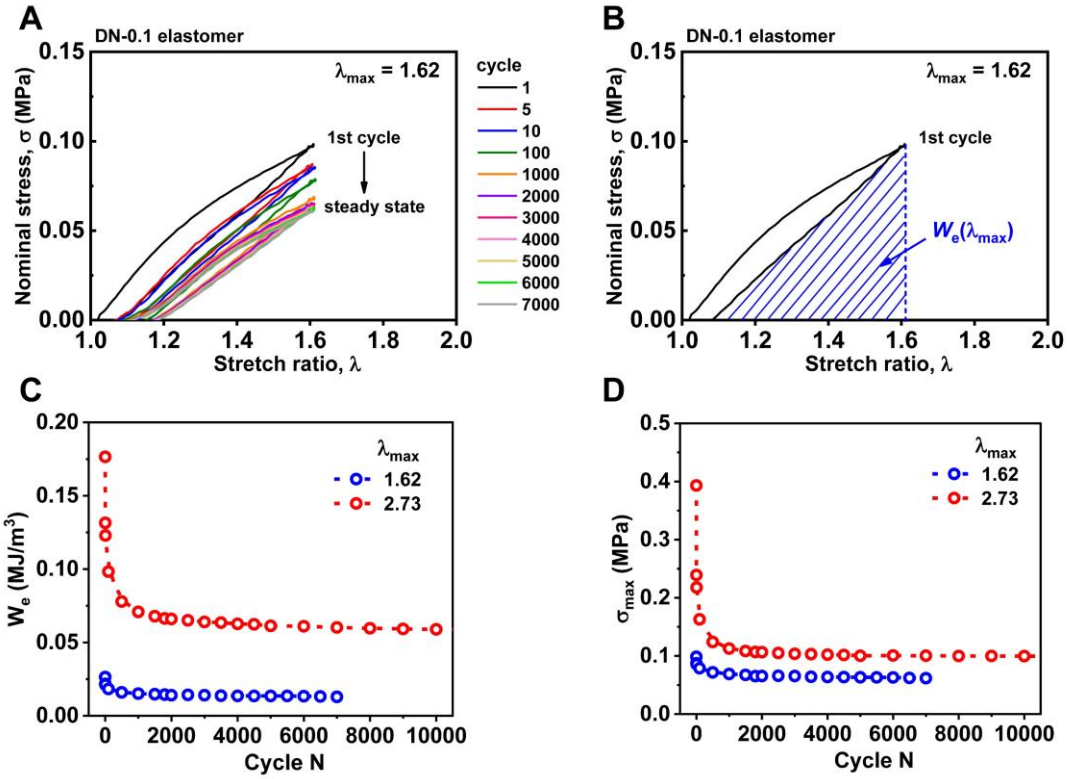

Figure S11. Characterizing the energy release rate G for DN-0.1 elastomer. (A) The loading-unloading curves to λ_{max} with increasing cycle N. The curves drop greatly at the beginning of the cycles and reach a steady state after thousands of cycles. (B) The area under the unloading curve shown by the blue hatch represents the elastic strain energy density $W_e(\lambda_{max})$. (C) Evolution of $W_e(\lambda_{max})$ and (D) σ_{max} with cycle N. The λ_{max}=1.62 and 2.73 are taken as examples. The $W_e(\lambda_{max})$ drops greatly at the beginning cycles and reaches a steady state after 2000 cycles. $W_e(\lambda_{max})$ at the 5000th cycle is used to estimate the energy release rate G by $G = W_e(\lambda_{max}) \times H_0$.